Title

Tunable Luminescence in Hybrid Cu(I) and Ag(I) Iodides

Journal

Inorganic Chemistry, 59(20)

ISSN

0020-1669 1520-510X

Authors

Wang, Shuxin

Morgan, Emily E

Vishnoi, Pratap

et al.

Publication Date

2020-09-29

DOI

10.1021/acs.inorgchem.0c02517

Peer reviewed

Tunable Luminescence in Hybrid Cu(I) and Ag(I) Iodides

Shuxin Wang,[1,2] Emily E. Morgan,[1] Pratap Vishnoi,[1] Lingling Mao,[1] Samuel M. L. Teicher,[1] Guang Wu,[3] Quanlin Liu,[2] Anthony K. Cheetham,[1,4] Ram Seshadri[1,3]*

[1]Materials Department and Materials Research Laboratory
University of California, Santa Barbara, California 93106, United States

[2]The Beijing Municipal Key Laboratory of New Energy Materials and Technologies,
School of Materials Sciences and Engineering
University of Science and Technology Beijing, Beijing 100083, China

[3]Department of Chemistry and Biochemistry
University of California Santa Barbara, California 93106, United States

[4]Department of Materials Science & Engineering
National University of Singapore, Singapore 117576 Singapore

ABSTRACT: Hybrid materials are increasingly demonstrating their utility across several optical, electrical, and magnetic applications. Cu(I) halide-based hybrids have attracted attention due to their strong luminescence in the absence of rare-earths. Here, we report three Cu(I) and Ag(I) hybrid iodides with 1,5-naphthyridine, and additional triphenylphosphine (Ph_3P) ligands. The compounds are built on (Cu/Ag)-I staircase chains or on a rhomboid Cu_2I_2 dimer and display intense and tunable luminescence. Replacing Cu with Ag, and adding the second kind of organic ligand (Ph_3P) tunes the emission color from red to yellow and results in significantly enhanced quantum yield. Density functional theory-based electronic structure calculations reveal the separate effects of the inorganic module and organic ligand on the electronic structure, confirming that bandgap, optical absorption and emission properties of these phosphors can be systemically and deliberately tuned by metal substitution and organic ligands cooperation. The emerging understanding of composition-structure-property relations in this family provides powerful design tools towards new compounds for general lighting applications.

INTRODUCTION

White light-emitting diodes (wLEDs) are capable of converting electricity to light effectively, thus considerably reducing overall electrical consumption worldwide.[1-4] Presently, high quality white light from wLEDs is predominantly produced by combining a blue-emitting InGaN/GaN chip with single or multicomponent blue light excitable phosphors.[5,6] Almost all current commercially employed phosphors in wLEDs are rare-earth (RE)-containing inorganic compounds, raising issues of supply, cost, and environmental damage.[7,8] Besides, their synthesis is generally energy intensive, requiring high temperatures and not permitting solution processing.[9-11] To tackle these issues, developing new types of RE-free, energy efficient, and solution processable phosphors is a significant endeavor.

With impressive structural diversity and great potential in optical, electrical, and magnetic applications, inorganic-organic hybrid materials are evolving into an important class of functional materials.[12-17] Among them, Cu(I) halide based hybrids have attracted attention due to their luminescence properties, and are regarded as promising for next generation lighting technologies.[18-25] Since the discovery of zero-dimensional $Cu_4I_4(pyridine)_4$, which is one of the most widely studied compounds, extensive research involving the varying of the inorganic modules and organic ligands has been carried out.[26-35] Combining the experimental results with density functional theory (DFT) calculations, it has been suggested that generally Cu(I) iodide based hybrids containing electron-donating organic ligands have higher quantum yields (QYs), pointing to the ability to tune optical properties by choosing suitable organic ligands.[20] In analogy to Cu(I), the closed-shell d^{10} electronic configuration enables structural diversity in Ag(I) compounds, including clusters, chains, and layer motifs.[36-40] Recently, highly luminescent tunable white-light emitting phosphors through the replacement of Cu by Ag in iodide based hybrids have been reported.[41] Nevertheless Ag(I) halide based hybrids are relatively less investigated compared to the related Cu(I) analogues.

With the aim of studying the effects of the metal and organic ligand on crystal structure, and to gain insights into composition-structure-property relations, we report three Cu(I) and Ag(I) semiconducting hybrid compounds obtained through judicious selection of metal cations and organic ligands. We report the preparation and characterization of three new compounds, 2D-Cu_2I_2(L) (**1**), 2D-

Ag_2I_2(L) (**2**), and 1D-$Cu_2I_2(Ph_3P)_2$(L) (**3**) (L= 1,5-naphthyridine, Ph_3P = triphenylphosphine). The compounds are built on (Cu/Ag)I staircase chains or on the rhomboid Cu_2I_2 dimer, and are intensely luminescent with tunable properties. Replacing Cu with Ag and incorporating a second kind of organic ligand (Ph_3P) in **1** not only tunes the emission color from red to yellow, but also results in enhanced quantum yield. DFT calculations point to the influence of the inorganic modules and organic ligands on the electronic structure, confirming that the bandgap, optical absorption and emission properties of these phosphors can be systemically and deliberately tuned by metal substitution and altering the organic ligand. The mechanism of photoluminescence is proposed based on their electronic structure and the interactions within the inorganic cluster. This work provides the foundations for understanding how metal substitution and ligand effects impact electronic structure and luminescence properties, helping in the rational design of functional hybrid phosphors for general lighting applications.

METHODS

Materials. CuI (98 %), AgI (99 %), triphenylphosphine were purchased from Spectrum Chemical and used as received. 1,5-naphthyridine (> 97 %) was purchased from Fisher Scientific and used as received.

Synthesis of 2D-Cu_2I_2(1,5-naphthyridine) (1). Single crystals of **1** were obtained by the layer method. CuI (38 mg; 0.2 mmol) was dissolved in a saturated aqueous KI solution (2 mL) which was placed in the reaction vial as the bottom layer. 1,5-naphthyridine (13 mg; 0.1 mmol) dissolved in ethanol (2 cm^3) was placed as the top layer. A mixture of deionized water (1 cm^3) and ethanol (1 cm^3) was used as the middle layer to separate the above two solutions. The reaction mixture in the closed vial was kept at room temperature to obtain orange plate-like crystals in 2 days. The crystals were collected by filtration, washed with ethanol and deionized water three times, respectively, and dried in a vacuum oven at 60 °C for 12 h.

Synthesis of 2D-Ag_2I_2(1,5-naphthyridine) (2). Single crystals of **2** were obtained by the layer method. 1,5-naphthyridine (13 mg; 0.1 mmol) in ethanol (2 mL) and AgI (47 mg; 0.2 mmol) in saturated aqueous KI solution (2 cm^3) were interlayered by 2 cm^3 mixture of deionized water (1 cm^3) and ethanol (1 cm^3). The vial was kept open at room temperature for 2 days to obtain yellow crystals. The crystals were collected by filtration and washed three times with ethanol and deionized water, respectively. The sample was dried in a vacuum oven at 60 °C for 12 h.

Synthesis of 1D-$Cu_2I_2(Ph_3P)_2$(1,5-naphthyridine) (Ph_3P = triphenylphosphine) (3). Single crystals of **3** were synthesized by starting from compound **1** with a solvothermal method. **1** (51 mg; 0.2 mmol) was dispersed in 5 cm^3 acetone and Ph_3P (65 mg, 0.25 mmol) dissolved in 1 cm^3 toluene was added slowly to the above solution. After stirring with a magnetic bar for 6 h, the mixture was heated at 160 °C for 12 h in a 23 cm^3 Teflon-lined autoclave in an oven. The autoclave was allowed to cool to room temperature which yielded orange crystals and powders of **3**. The sample was collected by filtration and washed with acetone and deionized water three times, respectively, and dried in a vacuum oven at 60 °C for 12 h.

Single crystal X-ray diffraction (SCXRD) and powder X-ray diffraction (PXRD). SCXRD data were collected at room temperature on a Bruker KAPPA APEX II diffractometer equipped with an APEX II CCD detector using a TRIUMPH monochromator with an Mo Kα source (λ = 0.71073 Å) and MX Optics. Crystal structures were solved using direct methods and refined by full-matrix least-squares on F^2 using the SHELXL-2014 program package.[42] PXRD patterns were collected using a PANalytical Empyrean powder diffractometer equipped with a Cu Kα radiation source (λ = 1.5418 Å).

Diffuse reflectance optical spectroscopy. A Shimadzu UV3600 UV-NIR Spectrometer was used to perform optical diffuse reflectance measurements. Data were collected in the wavelength range of 220 nm to 800 nm using $BaSO_4$ as the reference of 100 % reflectance. The Kubelka-Munk function was used for converting the reflectance spectra to optical absorption.

Computational details. Density functional theory (DFT) calculations were performed using the Vienna Ab initio Simulation Package[43-45] (VASP), version 5.4.4. The Perdew-Burke-Ernzerhof[46] (PBE) functional and projector-augmented wave[47,48] (PAW) pseudopotentials were used with a plane-wave cutoff energy of 500 eV. PAW potentials were chosen following the version 5.2 guidelines. Automatic *k*-mesh generation was used with a length parameter (R_k) of 40. Structure relaxation was performed using the DFT-D3 method[49] with Becke-Johnson damping.[50] For band-structure calculations, an appropriate *k*-path was generated using AFLOW[51,52], and band-structures were plotted and analyzed using Sumo.[53,54] Density of states (DOS) and crystal-orbital Hamilton population (COHP) analysis of pairwise bonding interactions were performed using the Local Orbital Basis Suite Towards Electronic-Structure Reconstruction (LOBSTER) package.[55-58]

Photoluminescence and internal Quantum Yield (QY) measurements. Photoluminescence emission (PL) and excitation (PLE) spectra, and QYs of powder samples were obtained on a Horiba FluoroMax-4 equipped with an integrating sphere using a 150 W continuous Xe arc lamp as excitation source at room temperature. All the PL and PLE spectra were calibrated by built-in correction files.

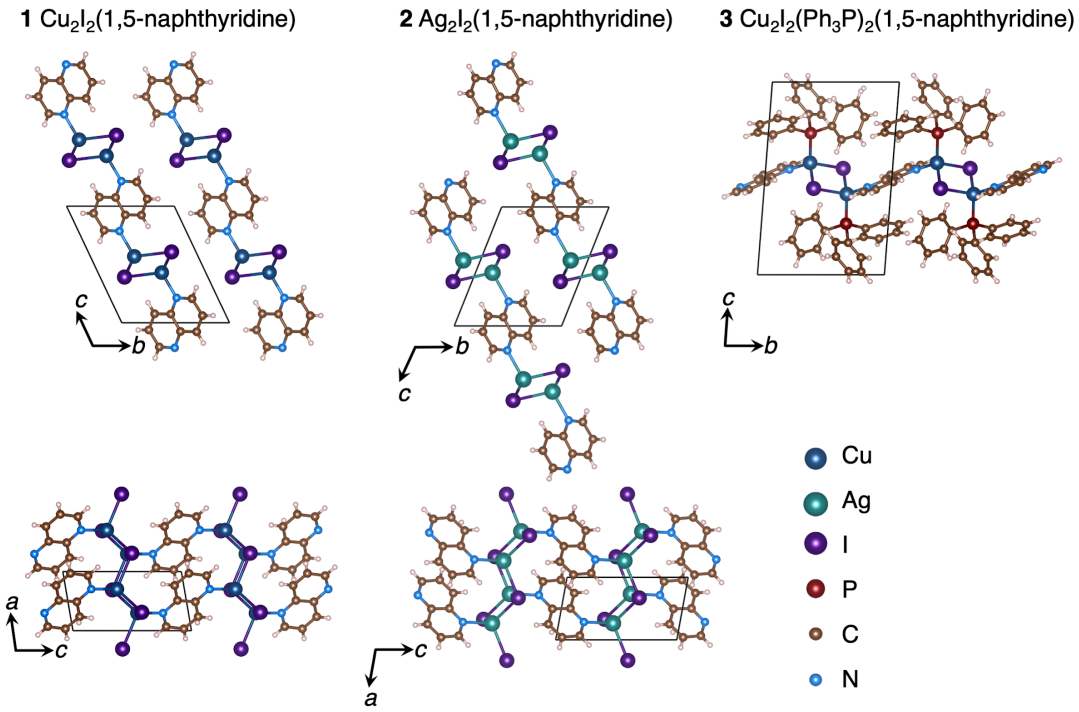

Figure 1. 2D crystal structures of **1** and **2** viewed along 2D layers (top) and same structure of **1** and **2** emphasizing one of the layers (bottom). 1D crystal structure of **3** viewed along the *a* axis, depicting one of the chains.

RESULTS AND DISCUSSIONS

All hybrid compounds presented here crystallize in the triclinic space group $P\bar{1}$. Crystallographic and structural refinements data are listed in Table 1 and S1-S7. **1** and **2** are built on one-dimensional Cu and Ag–I staircase chains, respectively. The adjacent 1D chains are further connected by two N atoms in 1,5-naphthyridine via Cu-N bonds in the case of **1** and Ag-N bonds in the case of **2**, forming two-dimensional layered structures (Figure 1). The metals (Cu or Ag) are tetrahedrally coordinated to one nitrogen atom of 1,5-naphthyridine and three iodine atoms. The shortest Cu–Cu and Ag–Ag distances are 2.7093 Å and 2.9277 Å in **1** and **2**, respectively.

Compound **3** was obtained from the reaction of **1** with triphenylphosphine. The addition of triphenylphosphine breaks the 1D Cu–I staircase into 0D rhomboid Cu_2I_2 motifs. The Cu_2I_2 motifs are further interconnected by 1,5-naphthyridine through Cu-N bonds forming a 1D chain structure, as illustrated in Figure 1. Cu is tetrahedrally coordinated to one N of 1,5-naphthyridine, one P atom of Ph_3P and two I of the inorganic motif. The shortest Cu–Cu distance is relatively longer (3.4524 Å) in this compound compared to **1** and **2**.

In regard to the dimensionality of the structures, we employ the I^nO^m classification scheme proposed by Cheetham *et al.* to describe the nature of the extended connectivity in these compounds.[59] The basis for the classification is the dimensionality of the connectivities *n* and *m* of the inorganic *I* and organic *O* components in the structure. **1** and **2** have infinite inorganic chains: $n = 1$, and the inorganic components are connected through the organic linker along *c* so $m = 1$, and these compounds are formally 2-dimensional ($n + m = 2$) with the classification I^1O^1. In contrast, the structure of **3** is characterized by Cu_2I_2 moieties linked back-to-back in chains by the 1,5-naphthyridene ligands, giving it the classification I^0O^1.

The phase purity of the bulk powder samples was examined by PXRD analysis, as shown in Figure 2. **1** and **2** are confirmed to be pure phases. For **3**, the additional peak at 10.6° originates from a small quantity of residual **1**.

It has been suggested that Cu–I based hybrid compounds have promising potential as alternative phosphors for wLEDs.[22,23] Studies have revealed that their photoluminescence can be attributed to one of three mechanisms: (i) halogen-to-ligand charge transfer (XLCT), (ii) metal-to-

Table 1. Crystallographic and structural refinements details for **1-3**.

compound	**1**	**2**	**3**
identification code	Cu_2I_2(1,5-naphthyridine)	Ag_2I_2(1,5-naphthyridine)	$Cu_2I_2(Ph_3P)_2$(1,5-naphthyridine)
empirical formula	C_4H_3NCuI	$C_8H_6N_2Ag_2I_2$	$C_{22}H_{18}NPCuI$
formula weight	256.52	599.69	517.78
temperature	294(2) K	110(2) K	293(2) K
wavelength	0.71073 Å	0.71073 Å	0.71073 Å
crystal system	triclinic	triclinic	triclinic
space group	$P\bar{1}$	$P\bar{1}$	$P\bar{1}$
unit cell dimensions	a = 4.311(4) Å	a = 4.592(2) Å	a = 8.355(2) Å
	b = 7.751(7) Å	b = 7.819(4) Å	b = 9.828(2) Å
	c = 9.098(8) Å	c = 9.325(4) Å	c = 14.196(4) Å
	α = 113.771(15) °	α = 107.798(8) °	α = 79.162(6) °
	β = 93.734(15) °	β = 104.368(8) °	β = 73.252(6) °
	γ = 102.296(15) °	γ = 101.968(8) °	γ = 65.168(5) °
volume (Å^3)	267.9(4)	293.9(2)	1010.0(5)
Z	2	1	2
density (calculated)	3.180 g/cm^3	3.457 g/cm^3	1.703 g/cm^3
absorption coefficient	9.688 mm^{-1}	8.547 mm^{-1}	2.694 mm^{-1}
F(000)	234	268	508
Crystal size (mm^3)	0.100 × 0.100 × 0.100	0.150 × 0.150 × 0.100	0.100 x 0.100 x 0.100
θ range for data collection	2.482° to 27.374°	2.434 to 26.421°	1.502° to 27.356°
reflections collected	2669	2230	9035
Independent reflections	1209	1210	4286
	[R(int) = 0.0311]	[R(int) = 0.0204]	[R(int) = 0.0246]
Completeness to θ = 25.242°	99.8 %	99.8 %	99.1 %
Max. and min. transmission	0.7455 and 0.4419	0.7454 and 0.5658	0.7454 and 0.6867
Refinement method	Full-matrix least-squares on F^2		
data / restraints / parameters	1209 / 0 / 64	1210 / 0 / 64	4286 / 0 / 235
Goodness-of-fit on F^2	1.017	1.088	0.992
final R indices	R1 = 0.0319,	R1 = 0.0367,	R1 = 0.0306,
[I > 2σ(I)]	wR2 = 0.0698	wR2 = 0.0872	wR2 = 0.0577
R indices [all data]	R1 = 0.0428,	R1 = 0.0472,	R1 = 0.0450,
	wR2 = 0.0750	wR2 = 0.0951	wR2 = 0.0629
largest diff. peak and hole	1.181 and -0.779 e.Å^{-3}	1.972 and -0.920 e.Å^{-3}	0.533 and -0.393 e.Å^{-3}

ligand charge transfer (MLCT), and (iii) Cu(I) d^{10}-d^9s^1 cluster centered (CC) transitions resulting from Cu–Cu interactions, especially when the Cu–Cu distance is shorter than 2.8 Å.[23] In order to gain insights into the compounds reported here and investigate their photoluminescent mechanisms, it is of significant importance to understand their optical and electronic properties. As shown in Figure 3, the estimated bandgaps of **1-3** are 2.28 eV, 2.92 eV, and 2.30 eV, respectively. To understand the influence of the structures and compositions on the electronic structures, DFT calculations were performed on all compounds. Figure 4 and Table 2 summarize the results of the band structure calculations. As expected, based on their structural similarities, **1** and **2** have qualitatively similar band structures, with the main difference being the significantly larger bandgap of **2**. This feature supports what was observed experimentally in the UV-vis absorption experiments. The difference in the bandgaps for **1** and **2** is likely derived from the fact that the valence band for **2** is much lower in energy than that of **1**. In the band structure for **3**, the calculated bandgap also qualitatively matches what was observed experimentally for this compound, in that it has a bandgap in between those of **1** and **2**. For all the structures, the states comprising the conduction band have a very narrow dispersion, resulting in very flat bands, which makes it difficult to judge direct versus indirect bandgaps in these materials. As expected for the PBE functional, the calculations significantly underestimate the value of the experimental bandgap. The Δ-sol method[60] was applied to the extended inorganic compounds **1** and **2** in order to better calculate their bandgaps. We can see that for **1** and **2**, the Δ-sol method does increase

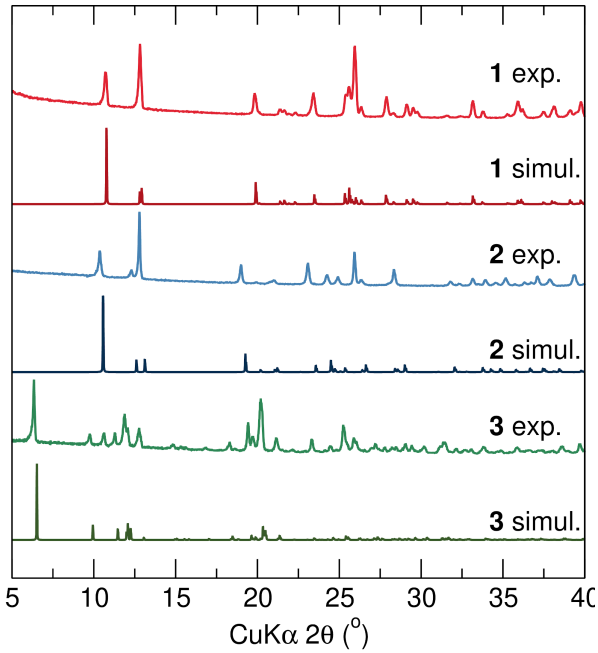

Figure 2. Simulated and experimental PXRD patterns of **1**-**3**. The additional peak at 10.6 ° in the experimental PXRD pattern of **3** originates from a small quantity of residual precursor **1**.

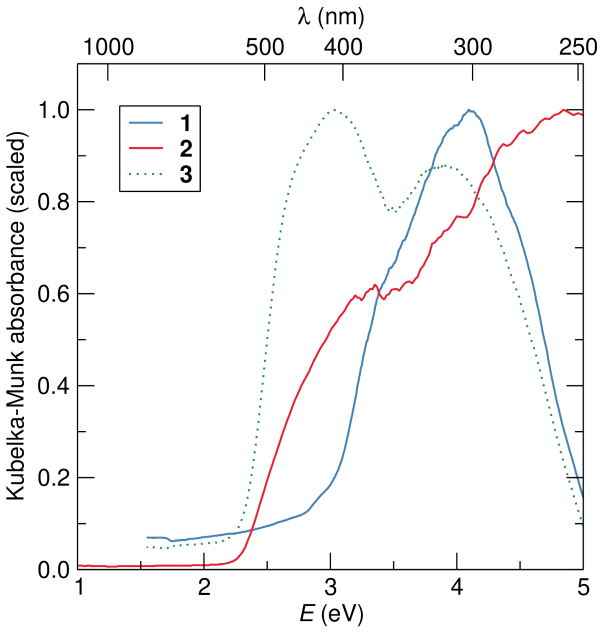

Figure 3. Optical absorption spectra of **1**-**3**. The estimated bandgaps of **1**-**3** are 2.28 eV, 2.92 eV, and 2.30 eV, respectively.

the calculated bandgap to yield values very close to what was observed experimentally. This method was not used for **3** due to the molecular nature of the structure, which is also seen in the extremely small dispersion of the bands.

As shown in Figure 5, the densities of states for these compounds reveal features similar to what has previously been observed in related systems.[20-22] In all compounds, the valence band maxima are dominated by contributions from the iodide 5p orbitals and metal d orbitals, with some small contributions from the nitrogen and carbon 2p orbitals, and phosphorous 3p orbitals in the case of **3**. The larger band gap of **2** over **1** is then explained by the lowered position of the d band of Ag compared with Cu. Additionally,

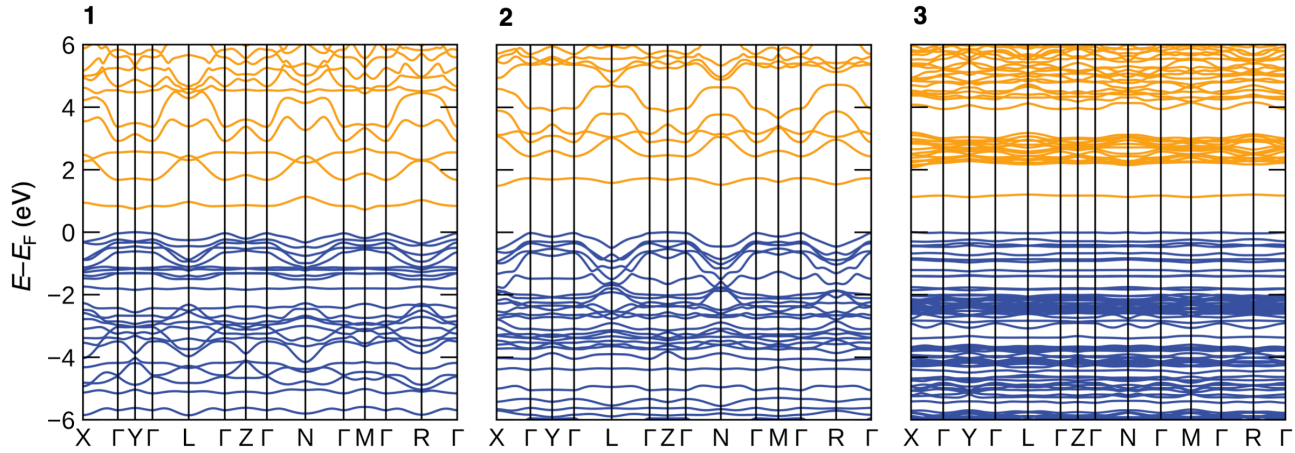

Figure 4. Panels depicting band-structures for **1**, **2**, and **3**, respectively, following a *k*-path through the high symmetry points in the Brillouin zone. **1** and **2** have similar band structures with the main difference being the significantly larger bandgap of **2**; **3** has a bandgap in between those of **1** and **2.**

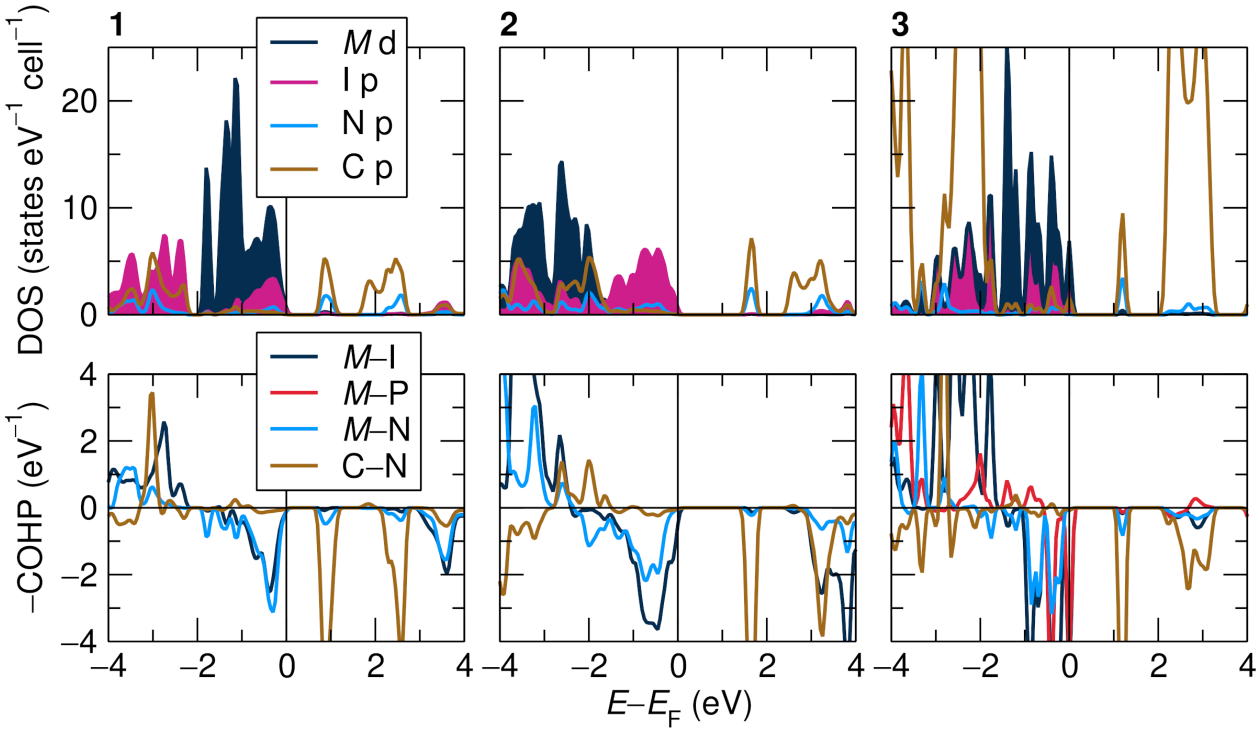

Figure 5. Top panels show the DOS for **1**, **2**, and **3**; Bottom panels show COHPs for **1**, **2**, and **3**. In all compounds, the valence band maxima are dominated by contribution from the iodide 5p orbitals and metal d orbitals, while the conduction band minima are composed of nitrogen and carbon 2p orbitals.

in all three cases the conduction band minima comprise nitrogen and carbon 2p orbitals. Therefore, judiciously selecting the metal and the organic ligands allows us to systematically tune the bandgaps of the resulting hybrids, and consequently their absorption and photoluminescence. The calculated DOS was also used for a COHP analysis. This method uses the DOS reconstruction in order to predict the amount of bonding or anti-bonding character present in different states. In the plots shown in Figure 5 (bottom), states that have positive values correspond to those that have more bonding character, while those with negative values will have more anti-bonding character. Using this analysis, we can see that the valence bands are mainly comprised of metal-iodide and metal-nitrogen antibonding interactions in **1** and **2**. In **3**, there are also metal-phosphorous antibonding states near the top of the valence band. In the conduction band, most of the states originate from carbon-nitrogen antibonding interactions, with some contribution from metal-nitrogen antibonding interactions.

Table 2. Summary of the band-structures for **1**–**3**.

Compound	Indirect gap (eV)	Direct gap (eV)	VBM (eV)	CBM (eV)	Δ-sol bandgap (eV)	Experimental bandgap (eV)
1	0.728	0.752 (Y)	2.920 (0, 0.48, 0)	3.648 (M)	2.26	2.28
2	1.489	1.687 (Z)	1.962 (0, 0, 0.48)	3.451 (X)	2.80	2.92
3	1.123	1.129 (X)	1.287 (X)	2.410 (M)	–	2.30

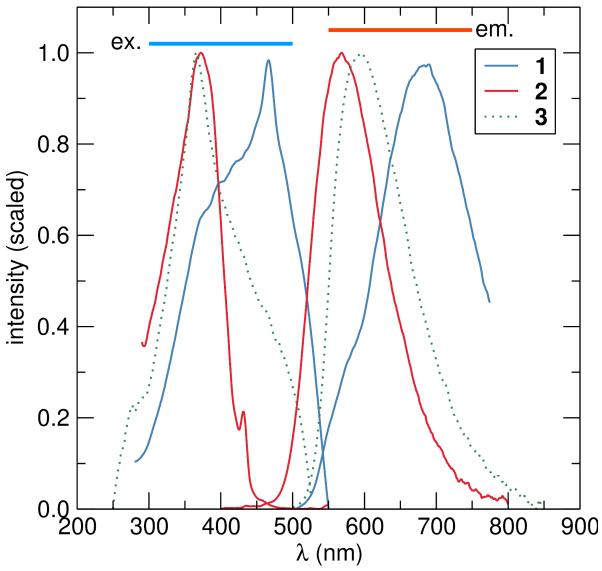

Figure 6. Photoluminescence excitation (PLE) and photoluminescence (PL) spectra of Cu_2I_2(1,5-naphthyridine) (**1**), Ag_2I_2(1,5-naphthyridine) (**2**) and $Cu_2I_2(Ph_3P)_2$(1,5-naphthyridine) (**3**).

The room temperature photoluminescence excitation (PLE) and photoluminescence (PL) spectra are shown in Figure 6. The PLE spectra of all the compounds monitored at their optimum emission wavelength exhibit broad band ranging from UV to blue light. The sharp peak at 467 nm in PLE spectrum of **1** is originated from the intensity fluctuations in Xe arc lamp. **1** shows a broad band emission peaked at 680 nm with a shoulder at 580 nm. **2** and **3** show single broad bands peaked at 566 nm and 595 nm, respectively. The emission colors of these hybrid compounds range from yellow to red. Detailed excitation energies and the corresponding emission peaks are listed in Table 3. Based on their electronic structures, and considering the short Cu–Cu (< 2.8 Å) and Ag–Ag (< 3.4 Å) distances,[22,61,62] we propose that the luminescent mechanism of **1** and **2** is a combination of XLCT, MLCT and CC transitions. For **3**, the shortest Cu–Cu distance, 3.4524 Å, is far longer than the sum of van der Waals radii of the two Cu atoms (2.8 Å), which points to the absence of a CC transition resulting from interactions within the inorganic cluster. Therefore, we suggest that the luminescence mechanism of **3** is a mixed XLCT/MLCT transition. The luminescence mechanisms for the compounds reported here resemble those that have been observed previously for CuI chain-based, Cu_2I_2 dimer-based, and Cu_4I_4 tetramer-based hybrid structures.[23] Compared with **1**, the emission bands of both **2** and **3** are blue shifted. For **2**, the replacement of Cu with Ag lowers the energy of the valence band and therefore increases the bandgap (Table 2), which tunes the emission color from red to yellow. For **3**, the Ph_3P incorporation lowers the energy of the valence band more than that of the conduction band, resulting in a greater bandgap (Table 2), which leads to the blue shift of the emission color. As a consequence, either Ag substitution or Ph_3P incorporation allows tuning of the valence band by controlling the dominant metal-main group bonding interactions, realizing tunable luminescence.

Table 3. Optical properties of **1**-**3**.

Compound	λ_{ex} (nm)	λ_{em} (nm)	Emission color	QY (%)
2D-Cu_2I_2(1,5-naphthyridine) (**1**)	370	680	red	1
2D-Ag_2I_2(1,5-naphthyridine) (**2**)	370	566	yellow	15
1D-$Cu_2I_2(Ph_3P)_2$(1,5-naphthyridine) (**3**)	365	595	yellow	19

1 has a relatively low QY of 1 %. For **2**, QY is improved to 15 % through replacing Cu by Ag. The observation of higher QYs for Ag complexes than the Cu analogue is not unusual and has been reported in several compounds, such as in $(Ag/Cu)_2I_2(Ph_3P)_2$(4,4'-bipyridine).[41,63] It has been suggested that the high QY (100%) of Ag(dbp)(P_2-nCB) [dbp = 2,9-di-n-butyl-1,10-phenanthroline, and P_2-nCB = nido-carborane-bis(diphenylphosphine)] is due to the presence of higher singlet excited states close to the S_1 excited states, which are also emitters.[64] On the basis of computation, Carbonell-Vilar *et al.* proposed that these states were not near to S_1 in [Ag(Xantphos)(4,4'-$(MeO)_2$-2,2'-bipy)]BF_4 [Xantphos: 4,5-bis-(diphenylphosphino)-9,9'-dimethylxanthene], and attributed the enhanced photoluminescence property of the Ag complex compared to its Cu analogue to the presence of non-emitting low-lying excited states with the Cu-O bonds, which do not exist in the Ag complex.[65] Consequently, the higher QYs for Ag complexes compared with the Cu analogues may be a consequence of the differences in excited states. However, from the DFT calculations presented here, it could also be suggested that the higher QY of **2** over **1** could arise due to the larger band gap, thereby avoiding some of the excitation being lost into the conduction band to non-radiative processes.

Adding the second ligand Ph_3P achieves the highest QY of 19 % for **3**, which can be attributed to its different inorganic module: the Cu_2I_2 dimer. This phenomenon is consistent with prior studies which showed that compounds built around the Cu_2I_2 rhomboid dimer or Cu_4I_4 cubane tetramer generally have higher luminescence efficiency than those built on CuI 1D chains.[66] This may result

from the more condensed structures of the Cu_2I_2 dimer and Cu_4I_4 tetramer, which typically reduces non-radiative processes and thereby achieves relatively higher quantum efficiencies. Our results show that both replacing Cu with Ag and adding a second kind of organic ligand (Ph_3P) can not only tune the emission color from red to yellow but also achieve higher QYs, thereby demonstrating two strategies for tuning the optical properties of CuI-based hybrid compounds: (i) metal substitution and (ii) ligand cooperation.

CONCLUSIONS

We report the preparation of three hybrid phosphors based around new 1D and 2D structures of Cu(I) and Ag(I) iodides with (Cu/Ag)I staircase chains or rhomboid Cu_2I_2 dimers. The compounds emit in the useful, yellow-red region with QYs ranging from 1 % to 19 %. Three types of luminescence mechanisms are proposed, depending on their electronic structures and interactions within the inorganic clusters. We have experimentally demonstrated that replacing Cu with Ag or adding the second spacer organic ligand (Ph_3P) can not only tune the emission color from red to yellow but also achieve higher QYs. DFT calculations further reveal the effects of the inorganic module and organic ligand on the electronic structures, confirming that the bandgaps and optical absorption and emission properties of these phosphors can be systemically and deliberately tuned by metal substitution and organic ligand cooperation. The realization of these new RE-free, solution-processable phosphors and the ability to tune their photoluminescence properties further improve our understanding of composition-structure-property relationships, and provide design tools for next-generation lighting applications.

ASSOCIATED CONTENT

Crystallographic details for Compound **1-3**. The Supporting Information is available free of charge via the Internet at http://pubs.acs.org.

AUTHOR INFORMATION

Corresponding Author

Ram Seshadri
Materials Department and Materials Research Laboratory, and Department of Chemistry and Biochemistry
University of California, Santa Barbara, California 93106, United States; orcid.org/0000-0001-5858-4027;
Email: seshadri@mrl.ucsb.edu

ACKNOWLEDGMENT

This work is supported by the U. S. Department of Energy, Office of Science, Basic Energy Sciences, under the grant DE-SC-0012541. SW thanks the China Scholarship Council for an State Scholarship Fund. PV thanks the Department of Science & Technology (DST), Govt. of India for an Overseas Post-doctoral Visiting Fellowship (Award No. JNC/AO/A.0610-1(3)/2018-03), managed by the Jawaharlal Nehru Centre for Advanced Scientific Research (JNCASR), Bangalore, India. This work made use of the facilities of the Materials Research Science and Engineering Center (MRSEC) at UC Santa Barbara supported by the National Science Foundation (DMR 1720256). SMLT has been supported by the NSF Graduate Research Fellowship Program under Grant No. DGE- 1650114.

REFERENCES

(1) Pimputkar, S.; Speck, J. S.; DenBaars, S. P.; Nakamura, S. Prospects for LED lighting. *Nat. Photonics.* **2009**, *3*, 180-182.

(2) George, N. C.; Denault, K. A.; Seshadri, R. Phosphors for solid-state white lighting. *Annu. Rev. Mater. Res.* **2013**, *43*, 481-501.

(3) Pattison, P. M.; Tsao, J. Y.; Brainard, G. C.; Bugbee, B. LEDs for photons, physiology and food. *Nature.* **2018**, *563*, 493-500.

(4) Wei, Y.; Xing, G. C.; Liu, K.; Li, G. G.; Dang, P. P.; Liang, S. S.; Liu, M.; Cheng, Z. Y.; Jin, D. Y.; Lin, J. New strategy for designing orangish-red-emitting phosphor via oxygen-vacancy-induced electronic localization. *Light: Sci. Appl.* **2019**, *8*, 1-9.

(5) Ye, S.; Xiao, F.; Pan, Y.; Ma, Y.; Zhang, Q. Phosphors in phosphor-converted white light-emitting diodes: Recent advances in materials, techniques and properties. *Mater. Sci. Eng., R.* **2010**, *71*, 1-34.

(6) Pust, P.; Weiler, V.; Hecht, C.; Tucks, A.; Wochnik, A. S.; Henss, A. K.; Wiechert, D.; Scheu, C.; Schmidt, P. J.; Schnick, W. Narrow-band red-emitting $Sr[LiAl_3N_4]:Eu^{2+}$ as a next-generation LED-phosphor material. *Nat. Mater.* **2014**, *13*, 891-896.

(7) Sprecher, B.; Daigo, I.; Murakami, S.; Kleijn, R.; Vos, M.; Kramer, G. J. Framework for resilience in material supply chains, with a case study from the 2010 Rare Earth Crisis. *Environ. Sci. Technol.* **2015**, *49*, 6740-6750.

(8) Tukker, A. Rare earth elements supply restrictions: market failures, not scarcity, hamper their current use in high-tech applications. *Environ. Sci. Technol.* **2014**, *48*, 9973-9974.

(9) Neeraj, S.; Kijima, N.; Cheetham, A. K. Novel red phosphors for solid state lighting; the system $NaM(WO_4)_{2-x}(MoO_4)_x$; Eu^{3+} (M=Gd, Y, Bi). *Chem. Phys. Lett*. **2004**, *387*, 2-6.

(10) Im, W. B.; George, N.; Kurzman, J.; Brinkley, S.; Mikhailovsky, A. A.; Hu, J,; Chmelka, B. F.; DenBaars, S. P.; Seshadri, R. Efficient and color-tunable oxyfluoride solid solution phosphors for solid-state white lighting. *Adv. Mater.* **2011**, *23*, 2300-2305

(11) Song, Z.; Liao, J.; Ding, X. L.; Liu, X. L.; Liu, Q. L. Synthesis of YAG phosphor particles with excellent morphology by solid state reaction. *J. Cryst. Growth.* **2013**, *365*, 24-28.

(12) Kagan, C.; Mitzi, D.; Dimitrakopoulos, C. Organic-inorganic hybrid materials as semiconducting channels in thin-film field-effect transistors. *Science.* **1999**, *286*, 945-947.

(13) Jain, P.; Ramachandran, V.; Clark, R. J.; Zhou, H. D.; Toby, B. H.; Dalal, N. S.; Kroto, H. W.; Cheetham, A. K. Multiferroic Behavior Associated with an

Order–Disorder Hydrogen Bonding Transition in Metal–Organic Frameworks (MOFs) with the Perovskite ABX_3 Architecture. *J. Am. Chem. Soc.* **2009**, *131*, 13625-13627.

(14) Saines, P. J.; Melot, B. C.; Seshadri, R.; Cheetham, A. K. Synthesis, structure and magnetic phase transitions of the manganese succinate hybrid framework, $Mn(C_4H_4O_4)$. *Chem.– Eur. J.* **2010**, *16*, 7579-7585.

(15) Furman, J. D.; Warner, A. Y.; Teat, S. J.; Mikhailovsky, A. A.; Cheetham, A. K. Tunable, ligand-based emission from inorganic-organic frameworks: a new approach to phosphors for solid state lighting and other applications. *Chem. Mater*. **2010**, *22*, 2255-2260.

(16) Thirumurugan, A.; Li, W.; Cheetham, A. K. Bismuth 2, 6-pyridinedicarboxylates: Assembly of molecular units into coordination polymers, CO_2 sorption and photoluminescence. *Dalton Trans*. **2012**, *41*, 4126-4134.

(17) Mao, L. L.; Guo, P. J.; Kepenekian, M.; Hadar, I.; Katan, C.; Even, J.; Schaller, R. D.; Stoumpos, C. C.; Kanatzidis, M. G. Structural Diversity in White-Light-Emitting Hybrid Lead Bromide Perovskites. *J. Am. Chem. Soc.* **2018**, *140*, 13078-13088.

(18) Peng, R.; Li, M.; Li, D. Copper(I) halides: A versatile family in coordination chemistry and crystal engineering. *Coordin. Chem. Rev.* **2010**, *254*, 1-18.

(19) Mazzeo, P. P.; Maini, L.; Petrolati, A.; Fattori, V.; Shankland, K.; Braga, D. Phosphorescence quantum yield enhanced by intermolecular hydrogen bonds in Cu_4I_4 clusters in the solid state. *Dalton Trans.* **2014**, *43*, 9448-9455.

(20) Zhang, X.; Liu, W.; Wei, G. Z.; Banerjee, D.; Hu, Z.; Li, J. Systematic approach in designing rare-Earth-free hybrid semiconductor phosphors for general lighting applications. *J. Am. Chem. Soc.* **2014**, *136*, 14230-14236.

(21) Liu, W.; Fang, Y.; Wei, G. Z.; Teat, S. J.; Xiong, K.; Hu, Z.; Lustig, W. P.; Li, J. A Family of Highly Efficient CuI-Based Lighting Phosphors Prepared by a Systematic, Bottom-up Synthetic Approach. *J. Am. Chem. Soc.* **2015**, *137*, 9400-9408.

(22) Fang, Y.; Liu, W.; Teat, S. J.; Dey, G.; Shen, Z. Q.; An, L.; Yu, D. C.; Wang, L.; O'Carroll, D. M.; Li, J. A Systematic Approach to Achieving High Performance Hybrid Lighting Phosphors with Excellent Thermal- and Photostability. *Adv. Funct. Mater.* **2017**, *27*, 1603444.

(23) Liu, W.; Fang, Y.; Li, J. Copper Iodide Based Hybrid Phosphors for Energy-Efficient General Lighting Technologies. *Adv. Funct. Mater.* **2018**, *28*, 1705593.

(24) Liu, Y.; Yiu, S.-C.; Ho, C.-L.; Wong, W.-Y. Recent advances in copper complexes for electrical/light energy conversion. *Coordin. Chem. Rev.* **2018**, *375*, 514-557.

(25) Xie, M.; Han, C.; Liang, Q.; Zhang, J.; Xie, G.; Xu, H. Highly efficient sky blue electroluminescence from ligand-activated copper iodide clusters: Overcoming the limitations of cluster light-emitting diodes. *Sci. Adv.* **2019**, *5*, eaav9857.

(26) Raston, C. L.; White, A. H. Crystal structure of the copper (I) iodide–pyridine (1/1) tetramer. *J. Chem. Soc., Dalton Trans.* **1976**, 2153-2156.

(27) Kyle, K. R.; Palke, W. E.; Ford, P. C. The photoluminescence properties of the copper (I) clusters $Cu_4I_4A_4$ (A= aromatic amine) in solution. *Coordin. Chem. Rev.* **1990**, *97*, 35-46.

(28) Kyle, K. R.; Ryu, C. K.; Ford, P. C.; DiBenedetto, J. A. Photophysical studies in solution of the tetranuclear copper (I) clusters $Cu_4I_4L_4$ (L= pyridine or substituted pyridine). *J. Am. Chem. Soc.* **1991**, *113*, 2954-2965.

(29) Vitale, M.; Palke, W. E.; Ford, P. C. Origins of the double emission of the tetranuclear copper (I) cluster Cu_4I_4 (pyridine)$_4$: An ab initio study. *J. Phys. Chem.* **1992**, *96*, 8329-8336.

(30) Chen, Y.; Li, H.-X.; Liu, D.; Liu, L.-L.; Li, N.-Y.; Ye, H.-Y.; Zhang, Y.; Lang, J.-P. Solvent effects on the assembly of $[Cu_2I_2]$-or $[Cu_4I_4]$-based coordination polymers: isolation, structures, and luminescent properties. *Cryst Growth Des.* **2008**, *8*, 3810-3816.

(31) Safko, J. P.; Kuperstock, J. E.; McCullough, S. M.; Noviello, A. M.; Li, X.; Killarney, J. P.; Murphy, C.; Patterson, H. H.; Bayse, C. A.; Pike, R. D. Network formation and photoluminescence in copper(I) halide complexes with substituted piperazine ligands. *Dalton Trans.* **2012**, *41*, 11663-11674.

(32) Khatri, N. M.; Pablico-Lansigan, M. H.; Boncher, W. L.; Mertzman, J. E.; Labatete, A. C.; Grande, L. M.; Wunder, D.; Prushan, M. J.; Zhang, W.; Halasyamani, P. S.; Monteiro, J. H.; Bettencourt-Dias, A.; Stoll, S. L. Luminescence and Nonlinear Optical Properties in Copper(I) Halide Extended Networks. *Inorg. Chem.* **2016**, *55*, 11408-11417.

(33) Cariati, E.; Bu, X. H.; Ford, P. C. Solvent- and vapor-induced isomerization between the luminescent solids $[CuI(4pic)]_4$ and $[CuI(4pic)]_\infty$ (pic = methylpyridine). The structural basis for the observed luminescence vapochromism. *Chem. Mater*. **2000**, 12, 3385-3391.

(34) Kang, Y.; Wang, F.; Zhang, J.; Bu, X. H. Luminescent MTN-type cluster-organic framework with 2.6 nm cages. *J. Am. Chem. Soc*. **2012**, 134, 17881-17884.

(35) Vitale, M.; Ryu, C. K.; Palke, W. E.; Ford, P. C. *Ab initio* studies of the copper(I) tetramers $Cu_4X_4L_4$ (X = I, Br, Cl). Effects of cluster structure and of halide on photophysical properties. *Inorg. Chem*. **1994,** 33, 561-566.

(36) Sampanthar, J. T.; Vittal, J. J. Silver-triphenylphosphine coordination polymers with linear spacer ligands. *Crystal engineering*. **2000**, *3*, 117-133.

(37) Chen, L.; Ma, J.; Chen, Q. H.; Feng, R.; Jiang, F. L.; Hong, M. C. A 2D silver-iodide-organic framework with both fluorescent and phosphorescent emissions. *Inorg. Chem. Commun.* **2012**, *15*, 208-211.

(38) Yang, D. D.; Xu, W. L.; Cao, X. W.; Zheng, S. J.; He, J. G.; Ju, Q.; Fang, Z. L.; Huang, W. Two silver coordination network compounds with colorful photoluminescence. *Inorg. chem.* **2016**, *55*, 7954-7961.

(39) Dosen, M.; Kawada, Y.; Shibata, S.; Tsuge, K.; Sasaki, Y.; Kobayashi, A.; Kato, M.; Ishizaka, S.; Kitamura, N. Control of Emissive Excited States of Silver(I) Halogenido Coordination Polymers by a Solid Solution Approach. *Inorg. Chem.* **2019**, *58*, 8419-8431.

(40) Yam, V. W.; Au, V. K.; Leung, S. Y. Light-Emitting Self-Assembled Materials Based on d^8 and d^{10} Transition Metal Complexes. *Chem. Rev.* **2015**, *115*, 7589-7728.

(41) Lin, F.; Liu, W.; Wang, H.; Li, J. Strongly emissive white-light-emitting silver iodide based inorganic-organic hybrid structures with comparable quantum

efficiency to commercial phosphors. *Chem. Commun.* **2020**, *56*, 1481-1484.

(42) Sheldrick, G. M. SHELXL-Integrated space-group and crystal-structure determination. *Acta Crystallogr., Sect. A: Found. Adv.* **2015**, 71, 3-8.

(43) Kresse, G.; Furthmüller, J. Efficiency of Ab-Initio Total Energy Calculations for Metals and Semiconductors Using a Plane-Wave Basis Set. *Comput. Mater. Sci.* **1996**, *6*, 15-50.

(44) Kresse, G.; Hafner, J. Ab initio molecular-dynamics simulation of the liquid-metal–amorphous-semiconductor transition in germanium. *Phys. Rev. B.* **1994**, *49*, 14251.

(45) Kresse, G.; Furthmüller, J. Efficient iterative schemes for ab initio total-energy calculations using a plane-wave basis set. *Phys. Rev. B.* **1996**, *54*, 11169.

(46) Perdew, J. P.; Burke, K.; Ernzerhof, M. Generalized gradient approximation made simple. *Phys. Rev. lett.* **1996**, *77*, 3865.

(47) Blöchl, P. E. Projector augmented-wave method. *Phys. Rev. B.* **1994**, *50*, 17953.

(48) Kresse, G.; Joubert, D. From ultrasoft pseudopotentials to the projector augmented-wave method. *Phys. Rev. B.* **1999**, *59*, 1758.

(49) Grimme, S.; Antony, J.; Ehrlich, S.; Krieg, H. A consistent and accurate ab initio parametrization of density functional dispersion correction (DFT-D) for the 94 elements H-Pu. *J. Chem. Phys.* **2010**, *132*, 154104.

(50) Grimme, S.; Ehrlich, S.; Goerigk, L. Effect of the damping function in dispersion corrected density functional theory. *J. Comput. Chem.* **2011**, *32*, 1456-1465.

(51) Curtarolo, S.; Setyawan, W.; Hart, G. L.; Jahnatek, M.; Chepulskii, R. V.; Taylor, R. H.; Wang, S.; Xue, J.; Yang, K.; Levy, O. AFLOW: an automatic framework for high-throughput materials discovery. *Comput. Mater. Sci.* **2012**, *58*, 218-226.

(52) Setyawan, W.; Curtarolo, S. High-throughput electronic band structure calculations: Challenges and tools. *Comput. Mater. Sci.* **2010**, *49*, 299-312.

(53) Ganose, A.; Jackson, A.; Scanlon, D. sumo: Command-line tools for plotting and analysis of periodic* ab initio* calculations. *J. Open. Source. Soft.* **2018**, *3*, 717.

(54) Ong, S. P.; Richards, W. D.; Jain, A.; Hautier, G.; Kocher, M.; Cholia, S.; Gunter, D.; Chevrier, V. L.; Persson, K. A.; Ceder, G. Python Materials Genomics (pymatgen): A robust, open-source python library for materials analysis. *Comput. Mater. Sci.* **2013**, *68*, 314-319.

(55) Maintz, S.; Deringer, V. L.; Tchougréeff, A. L.; Dronskowski, R. LOBSTER: A tool to extract chemical bonding from plane-wave based DFT. *J. Comput. Chem.* **2016**, *37*, 1030-1035.

(56) Maintz, S.; Deringer, V. L.; Tchougréeff, A. L.; Dronskowski, R. Analytic projection from plane-wave and PAW wavefunctions and application to chemical-bonding analysis in solids. *J. Comput. Chem.* **2013**, *34*, 2557-2567.

(57) Dronskowski, R.; Blöchl, P. E. Crystal orbital Hamilton populations (COHP): energy-resolved visualization of chemical bonding in solids based on density-functional calculations. *J. Phys. Chem.* **1993**, *97*, 8617-8624.

(58) Deringer, V. L.; Tchougréeff, A. L.; Dronskowski, R. Crystal orbital Hamilton population (COHP) analysis as projected from plane-wave basis sets. *J. Phys. Chem. A.* **2011**, *115*, 5461-5466.

(59) Cheetham, A. K.; Rao, C. N. R.; Feller, R. K. Structural diversity and chemistry trends in hybrid inorganic-organic framework materials. *Chem. Commun.* **2006**, *46*, 4780-4795.

(60) Chan, M.; Ceder, G. Efficient band gap prediction for solids. *Phys. Rev. Lett.* **2010**, *105*, 196403.

(61) Ford, P. C.; Cariati, E.; Bourassa, J. Photoluminescence properties of multinuclear copper (I) compounds. *Chem. Rev.* **1999**, *99*, 3625-3648.

(62) Hou, Q.; Jia, M.-J.; Zhao, J.-J.; Jin, J.; Yu, J.-H.; Xu, J.-Q. Two new 3-D photoluminescence metal–organic frameworks based on cubane Cu_4I_4 clusters as tetrahedral nodes. *Inorg. Chim. Acta.* **2012**, *384*, 287-292.

(63) Shibata, S.; Tsuge, K.; Sasaki, Y.; Ishizaka, S.; Kitamura, N. Directional Energy Transfer in Mixed-Metallic Copper (I)–Silver (I) Coordination Polymers with Strong Luminescence. *Inorg. Chem.* **2015**, *54*, 9733-9739.

(64) Yersin, H.; Czerwieniec, R.; Shafikov, M. Z.; Suleymanova, A. F. TADF material design: Photophysical background and case studies focusing on CuI and AgI complexes. *Chem. Phys. Chem.* **2017**, *18*, 3508-3535.

(65) Carbonell-Vilar, J. M.; Fresta, E.; Armentano, D.; Costa, R. D.; Viciano-Chumillas, M.; Cano, J. Photoluminescent Cu (I) vs. Ag (I) complexes: slowing down emission in Cu (I) complexes by pentacoordinate low-lying excited states. *Dalton Trans.* **2019**, *48*, 9765-9775.

(66) Liu, W.; Zhu, K.; Teat, S. J.; Dey, G.; Shen, Z.; Wang, L.; O'Carroll, D. M.; Li, J. All-in-One: Achieving Robust, Strongly Luminescent and Highly Dispersible Hybrid Materials by Combining Ionic and Coordinate Bonds in Molecular Crystals. *J. Am. Chem. Soc.* **2017**, *139*, 9281-9290.

For the Table of Contents

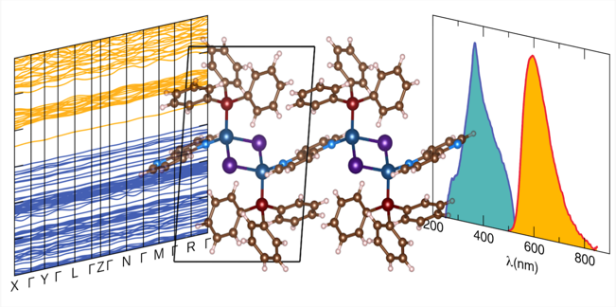

The brightly luminescent compound $Cu_2I_2(Ph_3P)_2$(1,5-naphthyridine) (Ph_3P = triphenylphosphine) has a structutre comprising neutral Cu_2I_2 moieties that form chains through coordination with the 1,5-napthyridine.

Supporting Information for

Tunable Luminescence in Hybrid Cu(I) and Ag(I) Iodides

Shuxin Wang,[1,2] Emily E. Morgan,[1] Pratap Vishnoi,[1] Lingling Mao,[1] Samuel M. L. Teicher,[1] Guang Wu,[3] Quanlin Liu,[2] Anthony K. Cheetham,[1,4] Ram Seshadri[1,3]*

[1]Materials Department and Materials Research Laboratory
University of California, Santa Barbara, California 93106, United States

[2]The Beijing Municipal Key Laboratory of New Energy Materials and Technologies,
School of Materials Sciences and Engineering
University of Science and Technology Beijing, Beijing 100083, China

[3]Department of Chemistry and Biochemistry
University of California Santa Barbara, California 93106, United States

[4]Department of Materials Science & Engineering
National University of Singapore, Singapore 117576 Singapore

*Email: seshadri@mrl.ucsb.edu

Table S1. Selected Bond lengths [Å] and angles [°] for **1**-**3**.

	1		**2**
Label	Bond length (Å)	Label	Bond length (Å)
I(1)-Cu(1)	2.6407(18)	Ag(1)-N(1)	2.322(6)
I(1)-Cu(1)#1	2.699(3)	Ag(1)-I(1)#1	2.8371(13)
I(1)-Cu(1)#2	2.741(2)	Ag(1)-I(1)	2.8399(12)
Cu(1)-N(1)	2.061(5)	Ag(1)-I(1)#2	2.9149(15)
Cu(1)-I(1)#1	2.699(3)	Ag(1)-Ag(1)#3	2.9277(16)
Cu(1)-Cu(1)#1	2.709(2)	I(1)-Ag(1)#4	2.8371(13)
Cu(1)-I(1)#3	2.741(2)	I(1)-Ag(1)#2	2.9149(15)
Label	Bond angle (°)	Label	Bond angle (°)
Cu(1)-I(1)-Cu(1)#1	60.97(4)	N(1)-Ag(1)-I(1)#1	110.29(15)
Cu(1)-I(1)-Cu(1)#2	106.44(7)	N(1)-Ag(1)-I(1)	108.41(15)
Cu(1)#1-I(1)-Cu(1)#2	82.08(4)	I(1)#1-Ag(1)-I(1)	107.96(4)
N(1)-Cu(1)-I(1)	111.91(14)	N(1)-Ag(1)-I(1)#2	106.45(15)
N(1)-Cu(1)-I(1)#1	112.50(14)	I(1)#1-Ag(1)-I(1)#2	118.83(3)
I(1)-Cu(1)-I(1)#1	119.04(4)	I(1)-Ag(1)-I(1)#2	104.40(3)
N(1)-Cu(1)-Cu(1)#1	138.16(15)	N(1)-Ag(1)-Ag(1)#3	128.18(15)
I(1)-Cu(1)-Cu(1)#1	60.58(7)	I(1)#1-Ag(1)-Ag(1)#3	60.72(4)

I(1)#1-Cu(1)-Cu(1)#1	58.46(5)	I(1)-Ag(1)-Ag(1)#3	123.12(4)
N(1)-Cu(1)-I(1)#3	107.21(15)	I(1)#2-Ag(1)-Ag(1)#3	58.10(4)
I(1)-Cu(1)-I(1)#3	106.44(7)	Ag(1)#5-I(1)-Ag(1)	107.96(4)
I(1)#1-Cu(1)-I(1)#3	97.92(4)	Ag(1)#5-I(1)-Ag(1)#2	61.18(3)
Cu(1)#1-Cu(1)-I(1)#3	114.40(7)	Ag(1)-I(1)-Ag(1)#2	75.60(3)
C(1)-N(1)-Cu(1)	118.5(4)	C(1)-N(1)-Ag(1)	118.0(5)
C(2)-N(1)-Cu(1)	123.4(4)	C(2)-N(1)-Ag(1)	124.0(5)

3

Label	Bond length (Å)	Label	Bond angle (°)
I(1)-Cu(1)	2.6929(7)	P(1)-Cu(1)-I(1)	107.23(3)
I(1)-Cu(1)#1	2.7004(7)	N(1)-Cu(1)-I(1)#1	114.68(7)
Cu(1)-N(1)	2.101(3)	P(1)-Cu(1)-I(1)#1	110.58(3)
Cu(1)-P(1)	2.2380(11)	I(1)-Cu(1)-I(1)#1	100.39(2)
Cu(1)-I(1)#1	2.7003(7)	C(5)-P(1)-Cu(1)	112.83(11)
	Bond angle (°)	C(11)-P(1)-Cu(1)	115.45(11)
Cu(1)-I(1)-Cu(1)#1	79.61(2)	C(17)-P(1)-Cu(1)	116.82(11)
N(1)-Cu(1)-P(1)	118.22(8)	C(1)-N(1)-Cu(1)	116.20(19)
N(1)-Cu(1)-I(1)	103.54(7)	C(2)-N(1)-Cu(1)	126.3(2)

Symmetry transformations used to generate equivalent atoms for

1: #1 -x+1,-y+1,-z+1 #2 x-1,y,z #3 x+1,y,z

2: #1 x+1,y,z #2 -x+1,-y+2,-z+1 #3 -x+2,-y+2,-z+1 #4 x-1,y,z

3: #1 -x+1,-y+1,-z+1

Table S2. Atomic coordinates (x 10^4) and equivalent isotropic displacement parameters ($Å^2$x 10^3) for **1**. U(eq) is defined as one third of the trace of the orthogonalized U^{ij} tensor.

	x	y	z	U(eq)
I(1)	3113(1)	7740(1)	6078(1)	30(1)
Cu(1)	7027(2)	5917(1)	4307(1)	39(1)
N(1)	7027(12)	6187(7)	2145(6)	30(1)
C(2)	4886(13)	4931(8)	745(7)	24(1)
C(3)	2365(14)	3443(9)	769(8)	33(1)
C(1)	9312(15)	7580(9)	2072(7)	33(1)
C(4)	307(15)	2197(9)	-615(8)	35(1)

Table S3. Atomic coordinates (x 10^4) and equivalent isotropic displacement parameters ($Å^2$x 10^3) for **2**. U(eq) is defined as one third of the trace of the orthogonalized U^{ij} tensor.

	x	y	z	U(eq)
Ag(1)	7137(2)	8413(1)	4481(1)	49(1)
C(1)	2594(17)	4460(10)	1927(9)	39(2)
C(2)	5774(15)	5752(9)	740(8)	31(1)
C(3)	8314(17)	7212(10)	835(9)	37(2)
C(4)	9096(17)	7113(10)	-483(9)	39(2)
I(1)	2973(1)	8240(1)	6269(1)	43(1)
N(1)	4917(13)	5849(8)	2063(7)	36(1)

Table S4. Atomic coordinates (x 10^4) and equivalent isotropic displacement parameters ($Å^2$x 10^3) for **3**. U(eq) is defined as one third of the trace of the orthogonalized U^{ij} tensor.

	x	y	z	U(eq)
I(1)	7772(1)	3896(1)	4479(1)	38(1)
Cu(1)	5053(1)	6536(1)	4189(1)	35(1)
P(1)	4762(1)	6671(1)	2652(1)	30(1)
N(1)	5818(3)	8126(3)	4539(2)	32(1)
C(2)	4662(4)	9486(3)	4922(2)	27(1)
C(5)	2721(4)	8234(3)	2406(2)	32(1)
C(10)	2330(5)	9626(3)	2724(2)	38(1)
C(11)	6602(4)	6948(3)	1664(2)	32(1)
C(17)	4647(4)	5029(3)	2285(2)	33(1)
C(1)	7574(5)	7828(3)	4306(3)	39(1)
C(3)	2789(4)	9867(3)	5184(2)	35(1)
C(15)	9824(5)	6070(4)	947(3)	50(1)
C(18)	5394(5)	4540(4)	1346(3)	41(1)
C(16)	8371(5)	5964(4)	1689(3)	42(1)
C(12)	6334(5)	8040(4)	894(3)	44(1)
C(4)	1666(5)	11209(3)	5573(3)	39(1)
C(6)	1501(5)	8131(4)	1971(3)	50(1)
C(19)	5275(5)	3287(4)	1113(3)	52(1)
C(9)	762(5)	10843(4)	2615(3)	48(1)
C(14)	9529(5)	7166(4)	180(3)	53(1)

C(8)	-448(5)	10710(4)	2203(3)	53(1)
C(13)	7790(5)	8156(4)	164(3)	55(1)
C(7)	-86(5)	9364(5)	1873(3)	59(1)
C(22)	3795(7)	4214(4)	2988(3)	63(1)
C(20)	4405(6)	2516(4)	1813(3)	62(1)
C(21)	3666(7)	2964(5)	2750(3)	75(2)

Table S5. Anisotropic displacement parameters ($Å^2 x\ 10^3$) for **1**. The anisotropic displacement factor exponent takes the form: $-2\pi^2[h^2 a^{*2} U^{11} + ... + 2 h k a^* b^* U^{12}]$

	U^{11}	U^{22}	U^{33}	U^{23}	U^{13}	U^{12}
I(1)	26(1)	31(1)	31(1)	12(1)	3(1)	6(1)
Cu(1)	41(1)	48(1)	29(1)	19(1)	8(1)	10(1)
N(1)	35(3)	31(3)	25(3)	13(2)	9(2)	9(2)
C(2)	28(3)	24(3)	23(3)	12(2)	5(2)	10(2)
C(3)	31(3)	41(4)	32(3)	20(3)	7(3)	12(3)
C(1)	39(3)	30(3)	29(3)	13(3)	4(3)	7(3)
C(4)	36(3)	35(3)	39(4)	23(3)	2(3)	4(3)

Table S6. Anisotropic displacement parameters ($Å^2 x\ 10^3$) for **2**. The anisotropic displacement factor exponent takes the form: $-2\pi^2[h^2 a^{*2} U^{11} + ... + 2 h k a^* b^* U^{12}]$

	U^{11}	U^{22}	U^{33}	U^{23}	U^{13}	U^{12}
Ag(1)	42(1)	53(1)	38(1)	7(1)	13(1)	3(1)
C(1)	40(4)	43(4)	40(4)	14(3)	19(3)	16(3)
C(2)	26(3)	34(4)	32(3)	10(3)	9(3)	10(3)
C(3)	35(4)	33(4)	35(3)	6(3)	10(3)	6(3)
C(4)	33(4)	39(4)	47(4)	18(3)	17(3)	7(3)
I(1)	38(1)	56(1)	49(1)	27(1)	23(1)	22(1)
N(1)	31(3)	41(3)	30(3)	10(3)	8(2)	9(3)

Table S7. Anisotropic displacement parameters ($Å^2 x\ 10^3$) for **3**. The anisotropic displacement factor exponent takes the form: $-2\pi^2[h^2 a^{*2} U^{11} + ... + 2\ h\ k\ a^*\ b^*\ U^{12}]$

	U^{11}	U^{22}	U^{33}	U^{23}	U^{13}	U^{12}
I(1)	37(1)	26(1)	43(1)	-4(1)	-1(1)	-8(1)
Cu(1)	43(1)	33(1)	34(1)	-7(1)	-10(1)	-15(1)
P(1)	34(1)	30(1)	28(1)	-4(1)	-6(1)	-16(1)
N(1)	33(2)	25(1)	36(2)	-5(1)	-6(1)	-11(1)
C(2)	34(2)	24(1)	25(2)	-1(1)	-8(1)	-12(1)
C(5)	35(2)	35(2)	26(2)	-2(1)	-1(1)	-17(1)
C(10)	44(2)	37(2)	37(2)	-6(2)	-6(2)	-19(2)
C(11)	37(2)	33(2)	31(2)	-8(1)	-6(1)	-18(1)
C(17)	42(2)	33(2)	32(2)	-5(1)	-12(2)	-19(1)
C(1)	38(2)	27(2)	44(2)	-11(1)	-1(2)	-10(1)
C(3)	39(2)	28(2)	41(2)	-2(1)	-11(2)	-16(1)
C(15)	35(2)	57(2)	56(3)	-13(2)	-4(2)	-17(2)
C(18)	49(2)	41(2)	39(2)	-7(2)	-5(2)	-24(2)
C(16)	43(2)	42(2)	43(2)	-4(2)	-9(2)	-19(2)
C(12)	41(2)	48(2)	39(2)	-1(2)	-8(2)	-16(2)
C(4)	29(2)	32(2)	51(2)	-4(2)	-3(2)	-10(1)
C(6)	52(2)	47(2)	57(3)	-16(2)	-22(2)	-15(2)
C(19)	64(3)	50(2)	47(2)	-22(2)	-7(2)	-24(2)
C(9)	51(2)	36(2)	44(2)	-4(2)	0(2)	-12(2)
C(14)	47(2)	68(3)	42(2)	-10(2)	7(2)	-31(2)
C(8)	40(2)	47(2)	49(2)	-1(2)	-6(2)	-1(2)
C(13)	51(3)	63(2)	41(2)	11(2)	-4(2)	-26(2)
C(7)	44(2)	68(3)	67(3)	-9(2)	-25(2)	-13(2)
C(22)	107(4)	67(3)	36(2)	-10(2)	-1(2)	-63(3)
C(20)	97(4)	49(2)	63(3)	-7(2)	-29(3)	-43(2)
C(21)	134(5)	79(3)	48(3)	0(2)	-11(3)	-83(3)